



UNIVERSITY OF LEEDS

This is a repository copy of *Oxygen-16 spectrum from tetrahedral vibrations and their rotational excitations*.

White Rose Research Online URL for this paper:
<http://eprints.whiterose.ac.uk/148593/>

Version: Accepted Version

Article:

Halcrow, CJ, King, C and Manton, NS (Cover date: April 2019) Oxygen-16 spectrum from tetrahedral vibrations and their rotational excitations. *International Journal of Modern Physics E*, 28 (4). 1950026. ISSN 0218-3013

<https://doi.org/10.1142/S0218301319500265>

(c) 2019, World Scientific Publishing Company. This is an author produced version of a paper published in the *International Journal of Modern Physics E*. Uploaded in accordance with the publisher's self-archiving policy.

Reuse

Items deposited in White Rose Research Online are protected by copyright, with all rights reserved unless indicated otherwise. They may be downloaded and/or printed for private study, or other acts as permitted by national copyright laws. The publisher or other rights holders may allow further reproduction and re-use of the full text version. This is indicated by the licence information on the White Rose Research Online record for the item.

Takedown

If you consider content in White Rose Research Online to be in breach of UK law, please notify us by emailing eprints@whiterose.ac.uk including the URL of the record and the reason for the withdrawal request.



eprints@whiterose.ac.uk
<https://eprints.whiterose.ac.uk/>

International Journal of Modern Physics E
 © World Scientific Publishing Company

Oxygen-16 Spectrum from Tetrahedral Vibrations and their Rotational Excitations

C. J. Halcrow

*School of Mathematics, University of Leeds,
 Leeds LS2 9JT, U.K.
 C.J.Halcrow@leeds.ac.uk*

C. King and N. S. Manton

*Department of Applied Mathematics and Theoretical Physics,
 University of Cambridge, Wilberforce Road, Cambridge CB3 0WA, U.K.
 ck402@cam.ac.uk and N.S.Manton@damtp.cam.ac.uk*

Received Day Month Year

Revised Day Month Year

A reinterpretation of the complete energy spectrum of the Oxygen-16 nucleus up to 20 MeV, and partly beyond, is proposed. The underlying intrinsic shape of the nucleus is tetrahedral, as in the naïve alpha-particle model and other cluster models, and A, E and F vibrational phonons are included. The A- and F-phonons are treated in the harmonic approximation, but the E-vibrations are extended into a two-dimensional E-manifold of D_2 -symmetric, four-alpha-particle configurations, following earlier work. This allows for the underlying tetrahedral configuration to tunnel through a square configuration into the dual tetrahedron, with the associated breaking of parity doubling. The frequency of an E-phonon is lower than in other models, and the first-excited 0^+ state at 6.05 MeV is modelled as a state with two E-phonons; this allows a good fit of the lowest 2^+ and 2^- states as excitations with one E-phonon. Rotational excitations of the vibrational states are analysed as in the classic work of Dennison, Robson and others, with centrifugal corrections to the rotational energy included. States with F-phonons require Coriolis corrections, and the Coriolis parameter ζ is chosen positive to ensure the right splitting of the 3^+ and 3^- states near 11 MeV. Altogether, about 80 states with isospin zero are predicted below 20 MeV, and these match rather well the more than 60 experimentally tabulated states. Several high-spin states are predicted, up to spin 9 and energy 30 MeV, and these match some of the observed high-spin, natural parity states in this energy range. The model proposed here is mainly phenomenological but it receives some input from analysis of Skyrmions with baryon number 16.

Keywords:

1. Introduction

For many decades there have been competing views of the intrinsic structure of the Oxygen-16 nucleus. In the naïve alpha-particle model, the nucleus is a cluster structure of four alpha particles at the vertices of a regular tetrahedron.¹ The

binding energy of Oxygen-16 and of several other small nuclei that contain a whole number of alpha particles can be interpreted in terms of the number of short bonds between them;^{2,3} for Oxygen-16 there are six bonds. In the shell model, on the other hand, there is an underlying spherically-symmetric potential, and the eight protons and eight neutrons fill all the available, lowest-lying 1s- and 1p-states, making the nucleus as a whole spherical, and magic. However, it is well known that the shell model picture is not completely incompatible with alpha-particle clustering in the Oxygen-16 ground state, and some extent of alpha clustering is confirmed in many experiments.^{4,5} For a review of alpha-particle clustering in light nuclei, see Ref. 6, and for recent discussions of the cluster structure in Oxygen-16, see Refs. 7, 8, 9. Some insight is afforded by *ab initio* calculations involving 16 nucleons with realistic 2-body and 3-body forces.¹⁰ Tetrahedral and square clusters of alpha particles appear to be favoured.

Of course, as the ground state of Oxygen-16 has $J^P = 0^+$, the mean particle density in this state is spherical in any model. However, a conceptual difference arises for the low-lying 3^- state at 6.13 MeV, which is known through its E3 decay strength to be a highly collective excitation. If the ground-state intrinsic shape is spherical, then this state is a vibrational excitation, perhaps with a tetrahedral character to account for the spin and parity. If the intrinsic shape is tetrahedral then this state is simply a rotational excitation.

The real challenge is to understand not just the ground state and a few low-lying excitations, but the entire known spectrum of excited states of Oxygen-16. A significant number of states can be described in terms of particle-hole excitations within the shell model. This was systematized by Brink and Nash;¹¹ see also D. J. Millener's theoretical foreword in Ref. 12. The single particle-hole states all have negative parity and describe a portion of the low-lying spectrum. To accurately model the known experimental energies, one must use techniques going beyond the independent particle version of the shell model, like the Tamm-Dacoff approach and the RPA.¹³ Even-parity states, including the 0^+ state at 6.05 MeV are less easily described in the shell model. Some of these states can be modelled as correlated 4-particle, 4-hole states,^{14,15} which can be interpreted as states with a mobile alpha particle that changes the underlying spherical shape. However, a systematic study of all excited states within the shell model would require a prohibitively large number of higher-energy 1-particle states to be activated, beyond the sd-shell. This leads us back to cluster models and collective excitations.

Our proposal, then, builds on the long history of modelling the excitation spectrum of Oxygen-16 in terms of vibrational excitations of a tetrahedral intrinsic structure. The many studies of possible tetrahedral structures in larger nuclei provide further stimulus.¹⁶⁻²⁰ Each vibrational state has an associated rotational band of rovibrational states, where the allowed spin/parities are controlled by the representation theory of the tetrahedral group. The earliest work on this, following Wheeler,¹ appears to be that of Dennison,²¹ who applied to the Oxygen-16 nucleus many insights gained from studying the spectra of tetrahedral molecules like

methane (CH_4). In particular, it was known that a tetrahedral structure of four alpha particles has three vibrational frequencies, associated with irreducible representations (irreps) A , E and F of the tetrahedral group^a. These irreps have, respectively, degeneracies 1, 2 and 3. Also known was that in the rotational excitations of a state with one vibrational F-phonon, it is important to take account of the (quantum) Coriolis effect. Dennison's work was followed up by Kameny²² and then by Robson.²³ By Robson's time, around 1980, the experimental states were much better known, so parameters like the vibrational frequencies and moments of inertia were better understood. Robson's fit of the spectrum led to a prediction of a 3^- state at 9.85 MeV that had not been seen. An experiment shortly afterwards at Florida State University confirmed that there was no such state,²⁴ which was a great disappointment, and struck a blow for this approach. However, the blow is not fatal, as we will show. The rovibrational model was revived by Bauhoff, Schultheis and Schultheis,²⁵ who found rotational bands for a number of different alpha-particle configurations, including tetrahedral, kite and chain clusters. These clusters are local minima of an energy function constructed from nucleon-nucleon forces. More recently, Bijker and Iachello²⁶ explored the consequences of novel, larger symmetry algebras that could predict the relative frequencies of the A , E and F vibrational modes. In particular, they considered the possibility that these frequencies are all equal at about 6 MeV, and they calculated the rotational excitations, successfully fitting about 10 known states. As in the earlier work, they drew attention to Coriolis contributions to the energy. However, there are clearly limitations to the success of their fit. An alternative rovibrational model is needed.

We previously considered the Oxygen-16 spectrum in Ref. 27. Our work developed from studies of Skyrmions, the solitons in an effective field theory of pions, whose topological charge is identified with baryon number (equivalently, atomic mass number).²⁸ In the Skyrme model a solution with baryon number 16, which is the basis for modelling Oxygen-16, has tetrahedral symmetry.^{29,30} We will not review Skyrmions in any detail here, as our rovibrational model for Oxygen-16 hardly depends on any variant of Skyrme's field theory. The main insight we have gained from Skyrmions is that in addition to the solution with baryon number 16 having tetrahedral symmetry, there is another solution of comparable energy with square symmetry, see Fig. 1.²⁹ The first solution mimics four alpha particles arranged as a tetrahedron, and the second, four alpha particles arranged as a square; the alpha particles are cube-like rather than point-like, and they merge to a small extent. However, we do not just consider these rigid intrinsic shapes. In Ref. 27 we showed that the two configurations are linked by a simple dynamical path within the Skyrme model, and we constructed a 2-parameter manifold of four-alpha-particle configurations that interpolates between these most symmetric solutions, and includes bent rhomb (rhomboidal) configurations.^{25,31} All the configurations parametrized by this manifold have D_2 symmetry. They can be regarded

^aWe shall be more careful later to distinguish the A_1 , A_2 , E , F_1 and F_2 irreps of T_d .

as alpha particles on four alternating vertices of a cuboid with variable shape, but fixed overall scale. Small deformations away from the tetrahedron, using the two parameters, correspond exactly to deformations of a tetrahedron by the doubly-degenerate vibrational E-mode, so we refer to the full 2-parameter configuration space as the E-manifold.

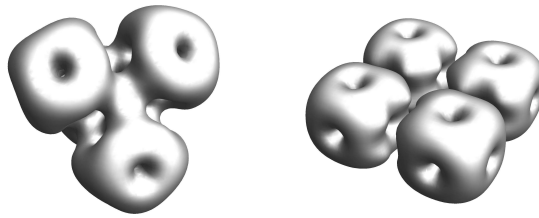


Fig. 1: Tetrahedral and square Skyrme configurations with baryon number 16. A contour of constant energy density of the Skyrme field is shown. The constituent cubes can be interpreted as alpha particles.

In Ref. 27 we quantized the E-manifold, taking account of the rotational degrees of freedom. The E-manifold has a structure like the surface of a deformed sphere with cubic symmetry, and the Hamiltonian on it has both kinetic and potential terms consistent with this symmetry. The Hamiltonian was not derived, so our results are phenomenological. However we found a number of states, and classified them by energy and spin/parity. In the bigger picture, they are the states of a rovibrational model, where there are any number of E-phonons, but no A- or F-phonons. The paper Ref. 27 was rather brief, but far more detail was presented in the PhD theses of the first two authors.^{32,33} There, the wavefunctions of more than a dozen E-manifold states were illustrated, and a start was made on extending the analysis to include the A- and F-phonons. This work is developed here, and we will clarify how the E-manifold states are interpreted in terms of E-phonons, which has not been done before. The Hamiltonian is not simply a harmonic oscillator in the neighbourhood of the tetrahedral solution, so the model gives insight into anharmonic aspects of vibrational E-phonons, but it is close enough to harmonic that multi-phonon states can easily be recognised. Being anharmonic, the model allows for dynamical transitions from the tetrahedron to its dual, via the square, so it captures in a rather sophisticated way the tunnelling between these configurations that Dennison considered, but modelled rather simply.²¹ Our E-manifold Hamiltonian predicts a significant lifting of the parity doubling, because the tunnelling probability is not negligible. In particular, in Ref. 27 we found a good fit to the splitting between the low-lying 6.92 MeV 2^+ and 8.87 MeV 2^- states of Oxygen-16. These are the lowest states with one E-phonon, and appear as degenerate in energy in Ref. 26, for example.

In this paper, we will describe a much more complete spectrum of states with several E-, A- and F-phonons. We assume that one F-phonon has energy about 6 MeV, and one A-phonon has energy about 12 MeV. An E-phonon has a smaller energy of about 3.5 MeV, although in practice the E-mode excitation energies are based on E-manifold quantum states that take into account the anharmonicity among E-modes, and tunnelling. The above ordering of frequencies is novel, because most earlier models treated the A-mode frequency as the lowest, but this ordering has more than one motivation. First, in a simple tetrahedral model of four equal bodies connected by six equal springs, the frequencies of the E-, F- and A-modes are in the proportions 1, $\sqrt{2}$ and 2.¹ A breather state, arising from exciting the A-mode, therefore has rather high energy. Second, in a related Skyrmion-inspired model of Carbon-12, a good understanding of several excited states was achieved.³⁴ There, the 0^+ ground state is based on an equilateral triangular arrangement of three alpha particles, and the 7.7 MeV Hoyle state, the lowest 0^+ excited state, arises from a vibrational excitation of the bending mode that connects the equilateral triangle to the straight chain of three alpha particles. The Hoyle state then has 2^+ and 4^+ rotational excitations, in agreement with data from Ref. 35. The 1-phonon breather excitation models the next 0^+ state of Carbon-12 at 9.9 MeV, whose rotational excitations would have spin/parity 2^+ , 3^- and 4^\pm , as in the Carbon-12 ground-state band. Using this, we can calibrate the A-mode frequency in Oxygen-16 by using the simple spring model between alpha particles and comparing with Carbon-12. The ratio of breather frequencies for a tetrahedron with six springs and a triangle with three springs is $2/\sqrt{3} \simeq 1.15$, so the 9.9 MeV breather state in Carbon-12 implies an 11.4 MeV breather state in Oxygen-16. Our A-mode frequency is close to this.

Oxygen-16 has a first-excited 0^+ state at 6.05 MeV, and in previous rovibrational models, this state was usually identified with the 1-phonon breather state, requiring the A-mode to have frequency 6.05 MeV. But in our model this state is instead a 2-phonon E-excitation, still with spin/parity 0^+ , which is why the E-mode frequency has to be near 3 MeV. The F-mode frequency is fixed by (uncontroversially) identifying the lowest 1^- state at 7.12 MeV as a 1-phonon F-excitation. The total energy of this state is approximately 6 MeV arising from the F-mode frequency, plus 1 MeV from the rotational energy.

The moment of inertia calibration for our model closely follows Robson.²³ The ground-state rotational band of Oxygen-16 has states associated with a rotating tetrahedron, with spin/parities 0^+ , 3^- , 4^+ , 6^\pm , 7^- , 8^+ and 9^\pm . Because a tetrahedron has the moment of inertia tensor of a spherical rotor, the rotational energies are of the form $BJ(J+1) - C(J(J+1))^2 + D(J(J+1))^3$ where B is Dennison's shorthand for $\frac{1}{2I}$, with I the moment of inertia; to fit the 3^- state at 6.13 MeV we set B to be 0.56 MeV. States beyond spin 3 have a significant centrifugal energy correction. The leading term $-C(J(J+1))^2$ is similar to Robson's, and we include the term $D(J(J+1))^3$ to ensure the rotational energy continues to increase up to

spin 9 and beyond^b. Robson chose $C = 3.2 \times 10^{-3}$ MeV, but we prefer a larger value $C = 4.5 \times 10^{-3}$ MeV combined with $D = 2.8 \times 10^{-5}$ MeV. We make small reductions to B when fitting rotational bands of vibrationally excited states – a standard correction in molecular physics,³⁶ reflecting the increased moment of inertia of a vibrating state. As in Robson’s analysis,²³ we find the ground-state rotational band incorporates the first-excited 6^+ state with energy 16.27 MeV, whereas the lowest 6^+ state with energy 14.82 MeV is part of the rotational band with one E-phonon. This band crossing is possible because of the difference between the moments of inertia in each band.

The final ingredient in our model is the Coriolis correction to the energies. This has been studied in depth by theoretical molecular chemists since the 1930s. Herzberg gives an illuminating review in Ref. 36, but the key original paper discussing Coriolis effects in tetrahedral molecules is by Johnston and Dennison.³⁷ The Coriolis effect arises because vibrational motion can carry an internal angular momentum, and this influences the total rotational energy. Vibrational excitations only involving A- and E-phonons have no Coriolis energy correction, but the F-band states – the states in the rotational band with just one F-phonon – do. A similar correction occurs when an F-phonon is combined with any number of A- and E-phonons. A rather different Coriolis correction occurs in the rotational band with two F-phonons. These corrections are reviewed in Section 3. Our most important observation is that the zeta factor, occurring in the Coriolis-corrected rotational energies, is not $\zeta = -0.5$. This is the value for four point-like alpha particles. (It is the value that emerges from an analysis of methane, when the central carbon atom is decoupled.) Dennison²¹ assumed that $\zeta = -0.5$ in the Oxygen-16 nucleus, and this assumption has been adopted by others.^{23,26} However, for extended alpha particle structures, as in the Skyrmion picture, where the alpha particles are partly merged and are not vibrating and rotating in the same way as hydrogen atoms do in methane, one can contemplate a different zeta value. Robson mentions this possibility in Ref. 38. Values of ζ in the range -1 to 1 are common for molecules with various geometries, and we find that a best fit occurs for ζ close to 0.2 . The main reason for our choice is to fit the splitting between the 11.08 MeV 3^+ state and the 11.60 MeV 3^- state in Oxygen-16. These are both modelled as F-band states, and the splitting is largely due to the Coriolis effect.

With these assumptions for our model and its parameters, we have calculated a rovibrational energy spectrum for the Oxygen-16 nucleus where essentially all states up to 20 MeV excitation energy are fitted moderately well. There are just over 60 such states with isospin 0 in the experimental tables,^{12,39} although there are uncertainties in the spin/parity and isospin assignments for several of the higher-energy states. The vibrational states we need to consider include up to four E-phonons, or two F-phonons, but at most one A-phonon. One new 4^- state is predicted below 15

^bThe parameters B and C are denoted B and D_s in Robson’s work.

MeV. There are no confirmed 6^- states in the tables, but our model predicts a few of these above 17 MeV. It also predicts several higher-spin states between 20 MeV and 30 MeV. Our model relies on seven basic parameters – the three vibrational frequencies ω_E , ω_F and ω_A , and the four rotational parameters B, C, D and ζ . In addition, there are some physically motivated adjustments to B that are fitted, depending on the vibrational state. Actually, this parameter count is a simplification because the E-vibrational energies are obtained from the quantization of the E-manifold, which has its own model, rather than by simply counting E-phonons.

2. E-manifold states

Here we consider the states that arise from quantization of the E-manifold. They include states in the ground-state rotational band, and in all the rotational bands associated with E-phonon vibrational excitations. The model for the E-manifold was introduced in Ref.²⁷ It is reviewed here, and we present the wavefunctions of the states, their energies and spin/parities in more detail than in Ref. 27. Most of these results appeared previously in Ref. 32, 33, but have been extended and updated here. We also clarify, for the first time, how the E-manifold states can be classified in terms of E-phonon counting.

The E-manifold is a model for four point alpha particles arranged in configurations with D_2 symmetry. The centre of mass is at the origin, and the D_2 symmetry is with respect to standard, Cartesian body-fixed axes. Let the Cartesian coordinates of one alpha particle be (x, y, z) ; the other three are then at $(x, -y, -z)$, $(-x, y, -z)$ and $(-x, -y, z)$, so the four particles are at alternating vertices of a cuboid. The scale size is fixed for each cuboid shape using a potential that disfavors the alpha particles from being too close together or too far apart. The E-manifold is therefore topologically a 2-sphere, parametrised by the direction of (x, y, z) . To visualise the E-manifold, we project a quarter of the 2-sphere onto a region of the complex plane, as shown in Fig. 2. Each point on the plane corresponds to a configuration of the four alpha particles, and the positions and orientations of the tetrahedron and square configurations, on the complex plane, are shown in Fig. 3.

The potential on the E-manifold has a minimum at the tetrahedral configuration, $(x, y, z) = (1, 1, 1)$ modulo scale, and there is a saddle point at the square configuration, $(x, y, z) = (1, 1, 0)$ modulo scale. The dynamics on the E-manifold is also arranged to force wavefunctions to approach zero as (x, y, z) approaches $(1, 0, 0)$ modulo scale, where the alpha particles form two pairs with a large separation between them.

The action of D_2 (π -rotations about the Cartesian axes) permutes the alpha particles, and since these are bosons, wavefunctions must be D_2 -invariant. The full symmetry group of the E-manifold, and of the dynamics on it, is the cubic group $O_h = O \times \mathbb{Z}_2$, with 48 elements. The non-trivial element of \mathbb{Z}_2 is inversion, $(x, y, z) \rightarrow (-x, -y, -z)$. The quotient of O by its normal subgroup D_2 gives the permutation group S_3 , which permutes the (unoriented) Cartesian axes. As a result,

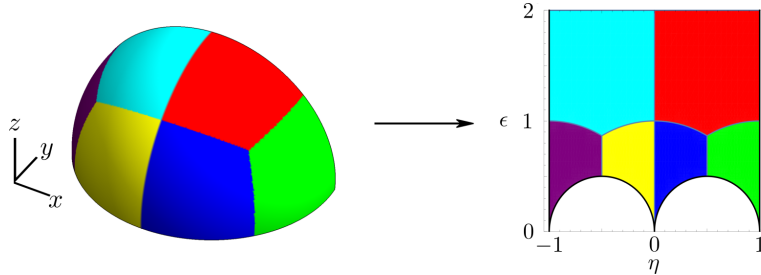
8 *C. J. Halcrow, C. King and N. S. Manton*


Fig. 2: The correspondence between the sphere and complex plane for one quarter of the E-manifold. Coloured regions are mapped to one another.

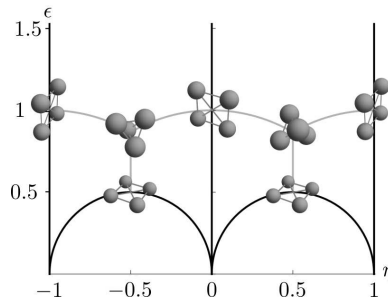


Fig. 3: The locations of some symmetric configurations on the complex plane. The balls represent alpha particles.

allowed wavefunctions on the E-manifold are classified by a representation of S_3 , and also a sign depending on how \mathbb{Z}_2 acts.

S_3 has three irreducible representations (irreps) – the 1-dimensional trivial irrep T , the 1-dimensional sign irrep S , and the 2-dimensional standard irrep St . Wavefunctions on the E-manifold are therefore labelled by species T^+ , S^+ , St^+ or T^- , S^- , St^- with an additional subscript n to denote the number of phonons in the state (which is described carefully below). The wavefunctions of species T and S are denoted by ψ , but those of species St have a 2-fold degeneracy, and the two linearly independent wavefunctions are denoted u and v .

Our Hamiltonian combines a kinetic term on the E-manifold (based on a hyperbolic metric on the 6-punctured sphere), and a potential that disfavors the alpha particles splitting into two pairs.²⁷ We have investigated numerically all the low-energy wavefunctions on the E-manifold. They are illustrated in Fig. 4, alongside their energies E_{vib} . The two lowest states ψ_{T0}^+ and ψ_{S0}^- have wavefunctions concentrated around the potential minima at the tetrahedron $(1, 1, 1)$ and its dual $(-1, -1, -1)$. Tunnelling between these is via the square saddle point. Wavefunc-

tions of the species S are constrained to vanish at the square while the species T wavefunctions have no such constraint. When the tunnelling amplitude is large, there is a relatively large energy gap between states that would otherwise be degenerate parity doubles. The lowest-energy wavefunctions, ψ_{T0}^+ and ψ_{S0}^- , have a small tunnelling amplitude, so their energy gap is small. Rotational excitations of these states jointly form the ground-state band. Higher-energy wavefunctions of species ψ_T^+ and ψ_S^- have a larger energy gap, because tunnelling is easier. The state ψ_{T2}^+ will be identified with the low-lying 0^+ state at 6.05 MeV. It is concentrated around both the tetrahedron and the square configurations. Physically, this state should be thought of as an admixture of a tetrahedron and a square. The lowest-energy states of species St are a positive-parity pair $u_1^+ + v_1^+$ and $u_1^+ - v_1^+$, and a negative-parity pair $u_1^- + v_1^-$ and $u_1^- - v_1^-$. The positive parity states are concentrated around the square configurations while the negative parity states are concentrated around the (prolate and oblate) bent rhombs. The rotational bands arising from these, with spin/parity $2^\pm, 4^\pm, 5^\pm, \dots$ can be interpreted as rotational excitations of the squares and rhombs.

A rather different classification is possible, and important here. Within O_h there is the 24-element subgroup T_d . This is the subgroup that preserves the configuration of four alpha particles at the vertices of a regular tetrahedron, where $(x, y, z) = (1, 1, 1)$. T_d acts nontrivially, but linearly, on small deformations of a configuration away from a regular tetrahedron. The group T_d has five irreps, the trivial and nontrivial 1-dimensional irreps A_1 and A_2 , the 2-dimensional irrep E , and the two 3-dimensional irreps F_1 and F_2 .⁴⁰ (The 3-dimensional irreps are often written as T_1 and T_2 .⁴¹)

Vibrational modes away from the tetrahedron in the direction of the E-manifold are 2-fold degenerate, and transform under the irrep E of T_d . Both the states ψ_{T0}^+ and ψ_{S0}^- are invariant under T_d , and are interpreted as states with no E-phonons, but the pair of states $u_1^+ + v_1^+$ and $u_1^+ - v_1^+$ are interpreted as degenerate 1-phonon states transforming under the irrep E , as are the pair $u_1^- + v_1^-$ and $u_1^- - v_1^-$. As T_d is a subgroup of O_h , each E-manifold state classified by an irrep of O_h is also classified by a T_d irrep. The states of species T^+ and S^- are in the A_1 irrep of T_d , the states of species T^- and S^+ are in the A_2 irrep, and the states of species St^+ and St^- are in the E irrep. No E-manifold states are classified by F_1 or F_2 . The T_d classification misses the \mathbf{Z}_2 label. This can be read off from the behaviour of the wavefunction under reflection in the vertical line splitting in half each subfigure of Fig. 4. If the wavefunction changes sign, then it is \mathbf{Z}_2 -odd.

It is known how multi-phonon states of a tetrahedron vibrating in the direction of the E-manifold transform under T_d . The phonons are bosonic, so one needs the decompositions of the symmetrised n th powers of the irrep E . For these, we should

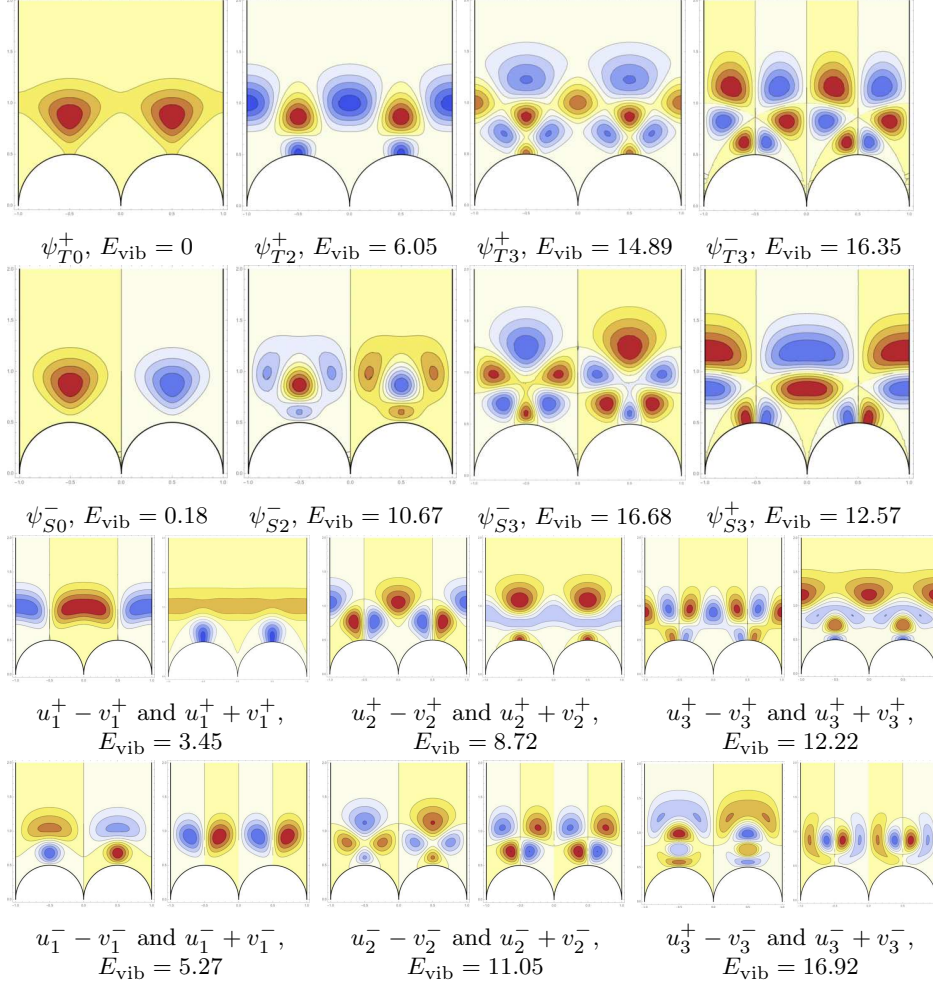
10 *C. J. Halcrow, C. King and N. S. Manton*


Fig. 4: The vibrational wavefunctions on the E-manifold. The plots show the wavefunction contours from -1 (blue) to $+1$ (red). The wavefunctions in the first row transform as the trivial irrep T , while those in the second row transform as the sign irrep S . The third (fourth) row transform as the standard irrep St with positive (negative) parity. The wavefunctions and axes are scaled for clarity. Energies are in MeV.

use the notation E_{symm}^n , but shorten this to E^n . These decompositions are,³⁶ p.127,

$$E^0 = A_1, \quad (1)$$

$$E^1 = E, \quad (2)$$

$$E^2 = A_1 \oplus E, \quad (3)$$

$$E^3 = A_1 \oplus A_2 \oplus E, \quad (4)$$

$$E^4 = A_1 \oplus 2E. \quad (5)$$

The dimension of E^n is $n + 1$, as expected for n -phonon states of a 2-dimensional harmonic oscillator. Combining the above algebraic information with the energy estimate that an n -phonon state has approximately n times the energy of a 1-phonon state, and inspecting the shape of the wavefunctions in Fig. 4 close to the tetrahedral configuration, one can classify these wavefunctions as follows. The wavefunctions $\psi_{T_0}^+$, $\psi_{S_0}^-$ are 0-phonon states, $u_1^+ \pm v_1^+$, $u_1^- \pm v_1^-$ are 1-phonon states, $\psi_{T_2}^+$, $\psi_{S_2}^-$ are 2-phonon A_1 states and $u_2^+ \pm v_2^+$, $u_2^- \pm v_2^-$ are 2-phonon E states. The wavefunctions $\psi_{T_3}^+$, $\psi_{S_3}^+$ are 3-phonon A_1 states, $\psi_{T_3}^-$, $\psi_{S_3}^-$ are 3-phonon A_2 states and $u_3^+ \pm v_3^+$, $u_3^- \pm v_3^-$ are 3-phonon E states. In all cases there is a pair of states distinguished by the \mathbf{Z}_2 label. This classification is verified by looking at the nodes of the wavefunctions, and comparing with harmonic oscillator states near the tetrahedral point expressed in (plane) polar coordinates. For example, 1-phonon states have one node, and 2-phonon A_1 states have a radial node. 3-phonon states have either six nodes in the angular direction, or a radial node and fewer than six nodes in the angular direction.

Classifying the E-manifold states in terms of E-phonons helps us compare our list of possible states, and their spin/parities, with the lists created by others. However, for the energy of an n -phonon state we use the E-manifold energies E_{vib} shown in Fig. 4, rather than the harmonic estimate $n\omega_E$. These are noticeably different, showing the importance of tunnelling through the square configuration.

Each E-manifold state has a band of rotational excitations. The allowed spin/parities J^P are those for which the decomposition of the $O(3)$ representation with spin/parity J^P contains the irrep of O_h classifying the E-manifold state (equivalently, a T_d irrep and a \mathbf{Z}_2 sign). These are essentially the same as the allowed spin/parities for vibrational states classified by T_d irreps (ignoring the \mathbf{Z}_2 sign), which are,³⁶ p.450,

$$A_1 \longrightarrow 0^+, 3^-, 4^+, 6^\pm, 7^-, 8^+, 9^\pm, \dots, \quad (6)$$

$$A_2 \longrightarrow 0^-, 3^+, 4^-, 6^\pm, 7^+, 8^-, 9^\pm, \dots, \quad (7)$$

$$E \longrightarrow 2^\pm, 4^\pm, 5^\pm, 6^\pm, 7^\pm, 8^\pm, 8^\pm, 9^\pm, \dots, \quad (8)$$

$$F_1 \longrightarrow 1^+, 2^-, 3^\pm, 4^\pm, 5^\pm, 5^+, 6^\pm, 6^-, 7^\pm, 7^\pm, 8^\pm, 8^\pm, 9^\pm, 9^\pm, 9^+, \dots, \quad (9)$$

$$F_2 \longrightarrow 1^-, 2^+, 3^\pm, 4^\pm, 5^\pm, 5^-, 6^\pm, 6^+, 7^\pm, 7^\pm, 8^\pm, 8^\pm, 9^\pm, 9^\pm, 9^-, \dots \quad (10)$$

E-manifold states only occur in the irreps A_1 , A_2 and E . The extra \mathbf{Z}_2 label for E-manifold states means that we can separate the positive and negative parity states, and assign them different vibrational energies. So, for example, the wavefunctions $\psi_{T_0}^+$, $\psi_{T_2}^+$, $\psi_{T_3}^+$ all allow positive parity A_1 states 0^+ , 4^+ , 6^+ , \dots , whereas the wavefunctions $\psi_{S_0}^-$, $\psi_{S_2}^-$, $\psi_{S_3}^-$ allow negative parity A_1 states 3^- , 6^- , 7^- , \dots . The wavefunction $\psi_{T_3}^-$ allows the unnatural parity A_2 state 0^- , and $\psi_{S_3}^+$ the unnatural parity A_2 state 3^+ . The wavefunctions $u_n^\pm \pm v_n^\pm$ allow E states 2^\pm , 4^\pm , 5^\pm , 6^\pm , \dots .

3. Rovibrational Energies

We now consider the rotational excitations of vibrational states, where each vibrational state is classified by the number of its A-, E- and F-phonons. We discuss all states with total energy up to 20 MeV, and states with spin 6 and higher up to 30 MeV. This means there are at most four E-phonons, two F-phonons, or one A-phonon. Combined vibrational states are also allowed, and include those combining one F- or A-phonon with one or two E-phonons. More precisely, the vibrational states are combinations of E-manifold wavefunctions with harmonic oscillator states for n_A A-phonons and n_F F-phonons, so the vibrational energy is the sum of the E-manifold energy E_{vib} and a contribution $n_A\omega_A + n_F\omega_F$. The E-manifold energy takes into account tunnelling between the tetrahedron and its dual, so we do not need to add an explicit tunnelling energy as in Ref. 23.

The rotational energy in a spin J state, including centrifugal corrections, is taken to be

$$E_{\text{rot}} = BJ(J+1) - C(J(J+1))^2 + D(J(J+1))^3. \quad (11)$$

In the ground-state band with no phonons, we set $B = 0.56$. For all E-manifold states having at least one E-phonon we set $B = 0.45$. This can be interpreted physically: the 0-phonon wavefunctions are concentrated at the tetrahedral configuration while the 1-phonon E-wavefunctions are concentrated at the square. The square has a larger moment of inertia and hence a smaller B . The same value $B = 0.45$ is used for states with one F-phonon or one A-phonon, and no E-phonons. For states with two F-phonons, combined E- and F-phonons, or combined E- and A-phonons, we set $B = 0.4$. This steady decrease of B as the number of phonons increases resembles the pattern used in molecular physics.³⁶ For the parameters C and D we choose the constant values $C = 4.5 \times 10^{-3}$ and $D = 2.8 \times 10^{-5}$. This ensures that the rotational energy increases approximately linearly with J between $J = 3$ and $J = 8$. The formula (11) is a simplified version of one proposed by Sood.^{42,43}

This is all we need to calculate the energy of states with no F-phonons. Mostly, these are multiple E-phonon states with no A-phonons, but some have a single A-phonon excitation transforming under the irrep A_1 . Since the A_1 irrep is trivial, the vibrational species $A_1 \otimes E^n$ allows for the same spins and parities as the E^n species.

There is a Coriolis energy correction for the F-band states, i.e. states with a single F-phonon and no A- or E-phonons. Each F-band state has an underlying E-manifold state with definite spin/parity situated in the ground-state rotational band, and based on either ψ_{T0}^+ or ψ_{S0}^- . This is combined using the usual Clebsch–Gordon angular momentum rules with a 1-phonon F-mode excitation that carries internal angular momentum 1 and (being triply-degenerate) transforms as the F_2 irrep of the T_d group. The states from the ground-state rotational band have spin/parities $0^+, 3^-, 4^+, 6^\pm, \dots$, whose rotational angular momentum is denoted by \mathbf{R} ; the intrinsic angular momentum of the F-phonon is denoted by \mathbf{l} . \mathbf{R} and \mathbf{l}

commute, and the total angular momentum is

$$\mathbf{J} = \mathbf{R} + \mathbf{1}. \quad (12)$$

The parity of the combined state is the opposite of the parity of the underlying rotational state, because the F-phonon has negative parity. The allowed combined states therefore have spin/parities (up to spin 9)

$$1_0^-, 2_3^+, 3_3^+, 4_3^+, 3_4^-, 4_4^-, 5_4^-, 5_6^\pm, 6_6^\pm, 7_6^\pm, 6_7^+, 7_7^+, 8_7^+, 7_8^-, 8_8^-, 9_8^-, 8_9^\pm, 9_9^\pm, 9_{10}^\pm, \quad (13)$$

where the usual spin/parity label J^P is supplemented by a subscript R to denote the underlying rotational angular momentum. R has one of the values $J + 1$, J or $J - 1$. Note that the J^P values occurring here are exactly the same as those one finds when considering an F-phonon as transforming under the F_2 irrep of T_d (see the list (10)).

The total rotational energy, including the Coriolis and centrifugal corrections, arises from the Hamiltonian^{36,37}

$$H_{\text{rot}} = B(\mathbf{J} - \zeta \mathbf{1})^2 - C(J(J+1))^2 + D(J(J+1))^3. \quad (14)$$

Expanding out, this is

$$H_{\text{rot}} = BJ(J+1) - 2B\zeta \mathbf{J} \cdot \mathbf{1} + 2B\zeta^2 - C(J(J+1))^2 + D(J(J+1))^3, \quad (15)$$

where we have set $l(l+1) = 2$ for internal angular momentum $l = 1$. (This expansion is valid even though \mathbf{J} and $\mathbf{1}$ do not commute, because the component pairs \mathbf{J}_i and $\mathbf{1}_i$ do commute.) By squaring eq. (12) we find $2\mathbf{J} \cdot \mathbf{1} = J(J+1) - R(R+1) + 2$, so the energy eigenvalues of H_{rot} are

$$E_{\text{rot}} = BJ(J+1) - 2B\zeta(1 - \zeta) - C(J(J+1))^2 + D(J(J+1))^3 + 2B\zeta \begin{cases} J+1 & \text{if } R = J+1, \\ 0 & \text{if } R = J, \\ -J & \text{if } R = J-1. \end{cases} \quad (16)$$

We now need to fix a calibration for ζ . As mentioned earlier, we will not make the standard choice, $\zeta = -0.5$. Instead, we fit ζ using the energies of the 3_3^+ and 3_4^- states in the F-band. The lowest F-band state should clearly be identified with the experimental 1^- state at 7.12 MeV, and spin 3 states are 4 MeV to 5 MeV above this. There is just one experimentally confirmed 3^+ state, at 11.08 MeV, and we identify this with the 3_3^+ state in the F-band. We identify the 3_4^- state in the F-band with the experimental 3^- state at 11.60 MeV (this is the first-excited 3^- state, as the lowest such state at 6.13 MeV is in the ground-state band, with no phonons). In our model, there are two sources for the 0.52 MeV energy splitting $E(3^-) - E(3^+)$. First, the underlying E-manifold states have an energy splitting of -0.18 MeV, because the $R = 4$ state with positive parity has underlying state ψ_{T0}^+ and the $R = 3$ state with negative parity has underlying state ψ_{S0}^- . The additional 0.70 MeV is from the Coriolis splitting between $J = 3$ states with $R = 4$ and

$R = 3$. This requires the calibration $2B\zeta = 0.175$, and as $2B = 0.9$ for the F-band, $\zeta = 0.194$. We will see below that this positive value for ζ gives reasonable energy splittings for several other states, up to spin/parity 5^\pm .

With ζ fixed, we note that the term $-2B\zeta(1 - \zeta)$ in eq. (16) is constant for the entire F-band and has value -0.14 MeV. This could be absorbed into the F-band phonon frequency, but we do not do this, as different constants occur in other bands, in particular the 2-phonon F^2 -band.

The rotational energy formula (16) extends to combined bands. It is known from molecular physics that ζ is unchanged for all bands of species $E^n \otimes F_2$. From the tetrahedral representation theory, it is known that the $E \times F$ band, with one E- and one F-phonon, transforms as $F_1 \oplus F_2$, and therefore the allowed spin/parities are parity doubles of the F-band states listed in (13). Again, there is an equivalent interpretation of these states. They are combinations of an underlying rotational state with one E-phonon, having spin/parity $2^\pm, 4^\pm, 5^\pm, \dots$, and an F-phonon with internal spin/parity 1^- . For example, in this band there are low-spin states with $J^P = 1^\pm, 2^\pm, 3^\pm$ all of which have $R = 2$, and further 3^\pm states with $R = 4$.

In the $E^2 \times F$ band, the calculation is similar. We recall that $E^2 = A_1 \oplus E$, so states with two E-phonons have underlying rotational states in the two lists (6) and (8). The angular momentum R of the underlying state combines with the 1^- of the F-phonon to give the total J^P . As the vibrational energy is quite high, we need only consider states with spins up to $J = 3$ in this band. We are less confident about our energies for states in the $E \times F$ and $E^2 \times F$ bands, because the relatively large amplitude of E-phonon(s) has an anharmonic effect on the F-phonon.

Finally, in the F^2 -band, things are a little different. States here have no E-phonons, so the underlying rotational states are those of the ground-state band with spin/parities $0^+, 3^-, 4^+, \dots$. As a single F-phonon has spin/parity 1^- , two F-phonons have internal spin/parity 0^+ or 2^+ . Therefore $l = 0$ or $l = 2$ in the F^2 -band. There are six states here, and this is consistent with the T_d decomposition $(F_2 \otimes F_2)_{\text{symm}} = A_1 \oplus E \oplus F_2$. For the $l = 0$ state there is no Coriolis effect, and the rotational energy (without the centrifugal corrections) is simply $BJ(J + 1)$. Here $B = 0.4$, the reduced value associated with having two F-phonons. For the $l = 2$ states, the rotational contribution to the energy is calculated starting from H_{rot} , the Hamiltonian in eq. (14), with $B = 0.4$ and $\zeta = -0.194$. The reversal of the sign of ζ follows the calculations in molecular physics,³⁷ although it may not be justified here. Expanding out H_{rot} we find rotational energies

$$\begin{aligned}
 E_{\text{rot}} = & BJ(J + 1) - 6B\zeta(1 - \zeta) - C(J(J + 1))^2 + D(J(J + 1))^3 \\
 & + 2B\zeta \begin{cases} 2J + 3 & \text{if } R = J + 2, \\ J + 1 & \text{if } R = J + 1, \\ 0 & \text{if } R = J, \\ -J & \text{if } R = J - 1, \\ -2J + 1 & \text{if } R = J - 2, \end{cases} \quad (17)
 \end{aligned}$$

where $R = 0, 3, 4, \dots$. States in the F²-band with energy below 20 MeV have spins no greater than $J = 4$. The parity of each state is the same as that of the underlying state, 0^+ , 3^- or 4^+ .

4. The Oxygen-16 Energy Spectrum

The theoretical energy spectrum of our model is plotted in Fig. 5, where states from each rotational band are displayed in a different colour. The total energy of each state is

$$E = E_{\text{vib}} + n_A \omega_A + n_F \omega_F + E_{\text{rot}}, \quad (18)$$

where E_{vib} is the underlying E-manifold energy, n_A and n_F the number of A- and F-phonons, with $\omega_A = 12.05$ MeV and $\omega_F = 6.55$ MeV their frequencies, and E_{rot} is the total rotational energy given by, respectively, eqs. (11), (16) or (17) in the cases of no F-phonons, one F-phonon or two F-phonons. We plot E against J . The spectrum is rather dense and so we plot it again in Fig. 6. Here, each spin/parity is considered separately and the figure also includes our proposed identification of model states with experimental states. Finally we tabulate the theoretical energies in Appendix A. The most important results are discussed below.

States with small fixed spin ($J \leq 4$) are generally ordered by their vibrational energy E_{vib} . Hence, the lowest-lying 0^+ , 3^- and 4^+ states all come from the E⁰ wavefunctions. They form the tetrahedral ground-state rotational band. Extrapolating this band to higher spins, using our energy formula, gives 6^\pm , 7^- , 8^+ and 9^\pm states. Of these, the natural parity states (having parity $(-1)^J$) have been observed at energies close to the predicted values, but their energies are not the lowest for those spins, because of band crossing. This was noted earlier by Robson, who identified the first-excited 6^+ state at 16.27 MeV as belonging to the tetrahedral ground-state band, although there is a lower 6^+ state at 14.82 MeV.

The next band is the E¹-band. Its lowest-energy states are a 2^+ state and a somewhat higher 2^- state with predicted energies close to those of the lowest observed states with these spin/parities. Experimentally, the energy splitting is 1.95 MeV, compared with 1.82 MeV in our model. The splitting is caused by the difference in vibrational energy due to tunnelling in the E-manifold. At higher spin, the E¹-band has the first-excited 4^+ state and the lowest predicted 4^- state, and the lowest 5^+ and 5^- states, always with the same splitting between the parity doubles. The lowest-energy 6^+ state also appears to be in this band, although its observed energy of 14.82 MeV is less than what our model predicts. The lowest observed 8^+ state is in this band too while the F-band gives rise to the lowest-energy 7^- state.

From spin 6 upwards, no unnatural parity states have yet been observed, but our model predicts several 6^- , 7^+ etc. states above 17 MeV. Each band has a selection of these, and their predicted energies are shown in the figures.

The E²-band is interesting, because in our model, the first-excited 0^+ state at 6.05 MeV is interpreted as belonging to this band. Because of the representation

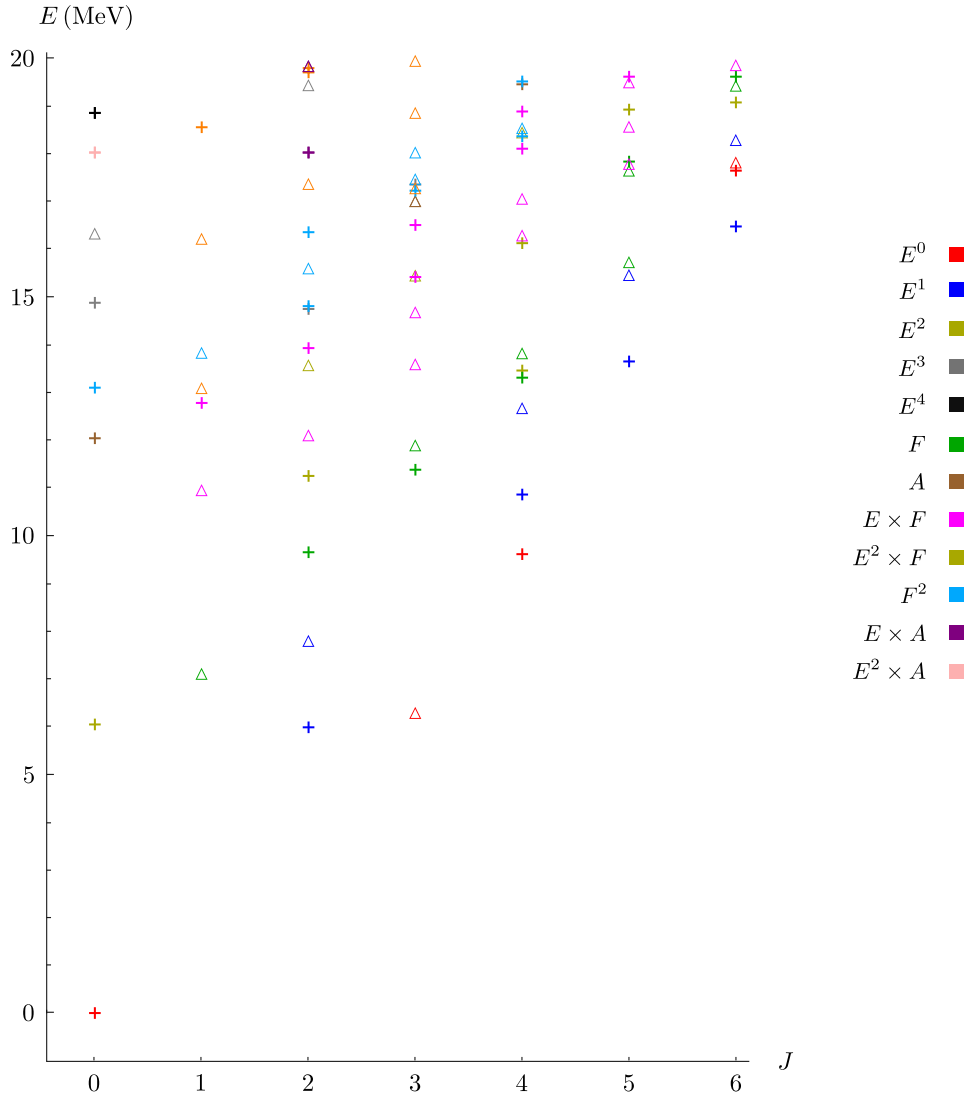


Fig. 5: Theoretical energy spectrum of our model. Each rotational band is coloured differently. Positive (negative) parity states are displayed as pluses (triangles).

decomposition $E^2 = A_1 \oplus E$, this band combines the spin/parities occurring in the ground-state E^0 -band with those in the E^1 -band, so it has states with spin/parities 0^+ , 3^- and 4^+ , and also 2^\pm and 4^\pm . The predicted 3^- state can be identified with the fourth-excited 3^- state at 15.41 MeV. This unexpectedly high energy occurs because of the relatively large vibrational energy of 10.67 MeV, and shows the importance of including the effect of tunnelling. Models which treat this state as a

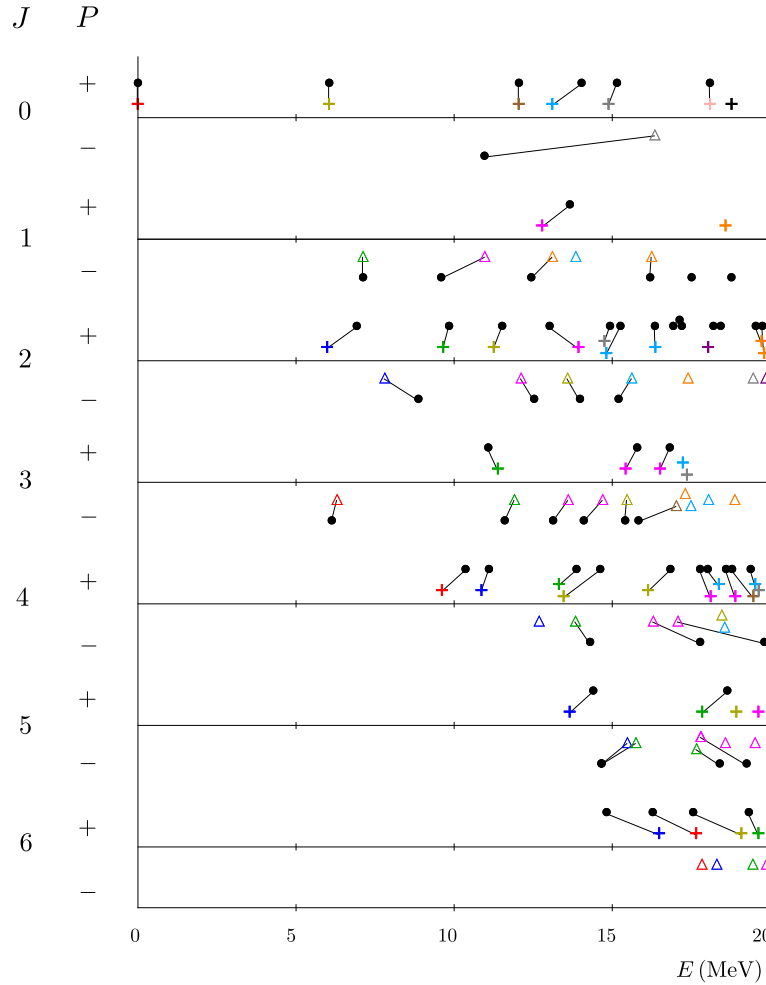


Fig. 6: Comparison between theoretical and experimental energies. Positive (negative) parity states of our model are displayed as pluses (triangles), and coloured as in Fig. 5 according to their rotational band assignment. Experimental states are displayed as black dots. Our identifications between theoretical and experimental states are shown by lines joining the states.

simple rotational excitation of the 0^+ state at 6.05 MeV give it an energy of 12 MeV or less. However, such an approach leads to too many 3^- states with low energy. The 2^\pm states in the E^2 -band match excited states with these spin/parities, and the two 4^+ states can be matched with the observed states either side of 15 MeV. The single 4^- state is predicted to lie above 18 MeV, close to where a couple of such states are observed.

The states in the F-band match experimental states quite well. For these, there is a significant contribution from the Coriolis effect. The band has the lowest 1^- state and the first-excited 2^+ state, then close together the lowest 3^+ state observed at 11.08 MeV and the first-excited 3^- state at 11.60 MeV. The 3^+ state is predicted to have energy higher than the 3^- state just from the difference in vibrational energy, but the Coriolis correction reverses this and makes the 3^+ state lower, to match the data. The 4^+ state matches an observed state, and the F-band also has a nearby 4^- state. So from the E^1 -band and F-band two 4^- states are predicted below 15 MeV, at 12.69 MeV and 13.84 MeV respectively, but just one is observed at 14.30 MeV. This is the first serious difference between the predictions of our model and what is observed. There is also some experimental uncertainty here,¹² although a state is clearly seen according to Kemper *et al.*,⁴⁴ and probably has unnatural parity. Our model clearly predicts two 4^- states in the 12-15 MeV range, although they could overlap. The model of Bijker and Iachello makes a similar prediction.²⁶ In the F-band there are two 5^- states and one 5^+ state. Further spin 5 states are predicted below 20 MeV, arising from the $E \times F$ band and E^2 -band. Compared to what has been seen in experiments, we predict two additional 5^+ states and three additional 5^- states. The observed 5^- peak at 14.66 MeV is unusually broad, and our model suggests it could arise from overlapping states in the E^1 - and F-bands with similar energies.

Let us now consider the higher-energy 0^+ states. It seems agreed by many authors that there is no 0^+ state at 11.26 MeV. (It is recorded in the experimental tables, but observed with a weak signal in just one experiment.⁴⁵) There are clearly observed 0^+ states at 12.05, 14.03 and 15.10 MeV. In our model we can match these to states in the F^2 -, E^3 - and A-bands. The predicted energies for the first two of these are 13.11 and 14.89 MeV, so it is most likely that the A-band state is at 12.05 MeV. This is the reason we have calibrated the A-mode, breather frequency to be 12.05 MeV, close to the value of 11.4 MeV estimated from the breather state of Carbon-12, as mentioned in the Introduction.

The E^3 -band also contains a 0^- state (because of the A_2 irrep in the decomposition of E^3), whose energy is predicted to be 16.35 MeV. This is far higher than the observed energy of 10.96 MeV for the lowest 0^- state, and is the worst prediction of our model. This problem was noted previously in Ref. 27. The wavefunction is shown in Fig. 4 (top right), and its energy is rather sensitive to the form of the potential on the E-manifold, away from the tetrahedron and square configurations where this wavefunction has to vanish. Possibly the energy can be lowered by adjusting the potential, but that would change all other energies, and we have not investigated the matter in detail.

The $E \times F$ band decomposes into F_1 and F_2 subbands. The states in the F_2 subband have the same spin/parities as those in the F-band but somewhat higher energies; the states in the F_1 subband have reversed parities. We will not describe in detail the states in this and in higher bands. There are a number of states with spins up to 5, below 20 MeV, that can be roughly matched to observed states, as

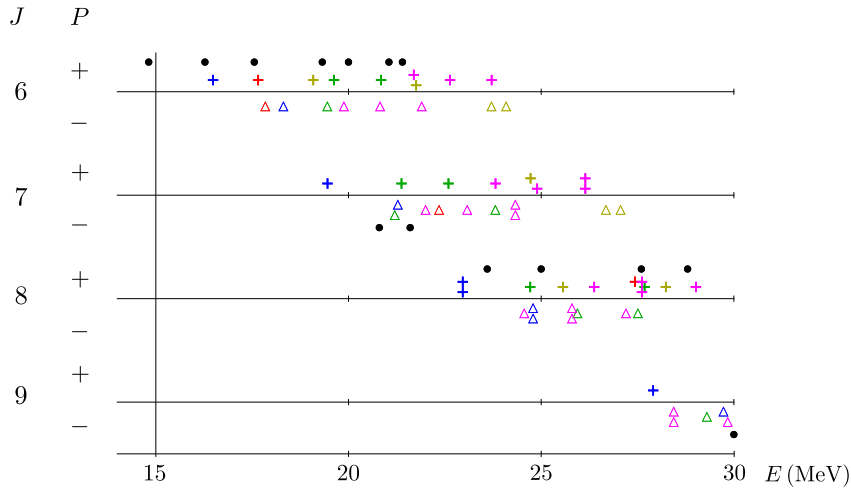


Fig. 7: Comparison between theoretical and experimental data for high-spin states with energies above 15 MeV, using the notation of Fig. 6. Only states from the E^0- , E^1- , E^2- , F- and $E \times F$ bands are displayed.

shown in Figs. 5 and 6. In particular, these bands give about the right number of 2^+ and 4^+ states to match the data. A number of 3^- states are predicted between 16 and 20 MeV, but none have so far been observed. A few 4^- states in the same energy range are also predicted.

3^+ states are an important check for our model as only three are observed lying below 20 MeV, at 11.08, 15.78 and 16.82 MeV. The third of these has uncertain spin and isospin. In our model, these three states arise from the F-band (one) and $E \times F$ band (two), at energies 11.39, 15.43 and 16.52 MeV. This indicates that the observed state at 16.82 MeV is definitely a 3^+ state with isospin 0. The $E \times F$ band also contains a single 1^+ state at 12.79 MeV, fairly close in energy to the observed state at 13.66 MeV, the only such state known. The next 1^+ state in our model is in the $E^2 \times F$ band and lies at 18.57 MeV. These rare spin states are especially important for comparing models. There are fifteen experimentally observed 2^+ states below 20 MeV. Hence it is difficult to verify (or falsify) a model using only 2^+ states, provided the model has lots of them. However an abundance of low-lying 1^+ or 3^+ states would be a significant failing.

The most interesting states with energy greater than 20 MeV are those with spin 6 or more, as some of these have been discovered recently,⁴⁶ and do not appear in the tables.¹² In fact, there has been significant debate within the literature about high-spin states of Oxygen-16. For example, Sanders *et al.* claimed to find an 8^+ state between 22 and 23 MeV in Ref. 47. Despite some effort in the years following, the state's existence was never corroborated by others^{48,49} and further, no other 8^+

state was discovered in this region. More recently, Freer *et al.* found at least three 8^+ states between 23 MeV and 30 MeV by studying Beryllium-8 decay channels.⁴⁶ These authors also discovered a 6^+ state at 21.2 MeV, close in energy to other 6^+ states at 21.4 MeV and 21.6 MeV seen in the experiments of Ref. 50 and Ref. 48 respectively. We will assume that these three states are all from a single broad resonance. There are two established 7^- states at 20.86 MeV and 21.62 MeV, and probably more at higher energy. There is also evidence of a 9^- state at around 30 MeV although its exact energy is uncertain.⁴⁹ Experimental work at these energies is difficult and we expect more states will be discovered as experimental techniques continue to improve. Fig. 7 shows the states predicted by our model, compared with the known experimental data, for 6^+ , 7^- , 8^+ and 9^- states. The states shown are from the E^0- , E^1- , E^2- , F- and $E \times F$ bands, although further 6^+ and 7^- states with energy below 30 MeV are likely to arise from higher bands. The model predicts a similar number of unnatural parity states, but none have yet been observed. Our high-spin spectrum is dense with states and includes numerous degeneracies. This is characteristic of any cluster model. Since states at this energy often appear as broad resonances, it may be difficult to experimentally distinguish individual states which are nearby in energy. Regardless, our model predicts a high-spin spectrum just as dense and complex as what is seen at lower energies.

Overall, the model successfully describes approximately 70 states in the observed spectrum of Oxygen-16, with most of the energy predictions matching measured energies within about 1 MeV. Exceptionally, the predicted energy for the lowest 0^- state is about 5 MeV too high. A number of 3^- and 4^- states just below 20 MeV are predicted, and numerous unnatural parity states with high spin should exist, starting with a 6^- state in the ground-state band between 17 MeV and 18 MeV. Perhaps our most important prediction is the existence of a further 4^- state around 13 MeV. Finding such a state would help confirm the tetrahedral cluster model approach to the Oxygen-16 nucleus, and the importance of considering the global structure of the E-manifold and the effect of tunnelling.

Acknowledgements

This work has been partially supported by STFC consolidated grant ST/P000681/1. CJH is supported by The Leverhulme Trust as an Early Careers Fellow. CK was supported by an STFC studentship.

References

1. J. A. Wheeler, Molecular viewpoints in nuclear structure. *Phys. Rev.* **52** (1937) 1083.
2. W. Wefelmeier, Ein geometrisches Modell des Atomkerns. *Zeit. f. Phys.* **A107** (1937) 332.
3. L. R. Hafstad and E. Teller, The alpha-particle model of the nucleus. *Phys. Rev.* **54** (1938) 681.
4. J. K. Perring and T. H. R. Skyrme, The alpha-particle and shell models of the nucleus. *Proc. Phys. Soc.* **A69** (1956) 600.

5. A. Volya and Y. M. Tchuvil'sky, Nuclear clustering using a modern shell-model approach. *Phys. Rev.* **C91** (2015) 044319.
6. Y. Fujiwara *et al.*, Comprehensive study of structure of light nuclei – chapter 2: comprehensive study of alpha-nuclei. *Prog. Theor. Phys. Suppl.* **68** (1980) 29.
7. Y. Kanada-En'yo, Tetrahedral 4α and $^{12}\text{C} + \alpha$ cluster structures in ^{16}O . *Phys. Rev.* **C96** (2017) 034306.
8. M. Freer, H. Horiuchi, Y. Kanada-En'yo, D. Lee and U.-G. Meißner, Microscopic clustering in light nuclei. *Rev. Mod. Phys.* **90** (2018) 035004.
9. T. Fukui, Y. Kanada-En'yo, K. Ogata, T. Suhara and Y. Taniguchi, Investigation of spatial manifestation of α clusters in ^{16}O via α -transfer reactions. *Nucl. Phys.* **A983** (2019) 38.
10. E. Epelbaum, H. Krebs, T. A. Lähde, D. Lee, U.-G. Meißner and G. Rupak, *Ab initio* calculation of the spectrum and structure of ^{16}O . *Phys. Rev. Lett.* **112** (2014) 102501.
11. D. M. Brink and G. F. Nash, Excited states in Oxygen 16. *Nucl. Phys.* **40** (1963) 608.
12. D. R. Tilley, H. R. Weller and C. M. Cheves, Energy levels of light nuclei $A = 16 - 17$. *Nucl. Phys.* **A564** (1993) 1.
13. J. Suhonen, *From Nucleons to Nucleus*. Springer, Berlin Heidelberg, 2007.
14. W. H. Bassichis and G. Ripka, A Hartree-Fock calculation of excited states of O^{16} . *Phys. Lett.* **15** (1965) 320.
15. J. M. Irvine, C. D. Latorre and V. F. E. Pucknell, The structure of ^{16}O ; A review of the theory. *Adv. in Phys.* **20:88** (1971) 661.
16. S. Takami, K. Yabana and M. Matsuo, Tetrahedral and triangular deformations of $Z = N$ nuclei in mass region $A \sim 60 - 80$. *Phys. Lett.* **B431** (1998) 242.
17. J. Dudek, A. Goźdź, N. Schunck and M. Miśkiewicz, Nuclear tetrahedral symmetry: possibly present throughout the periodic table. *Phys. Rev. Lett.* **88** (2002) 252502.
18. S. Tagami, Y. R. Shimizu and J. Dudek, Tetrahedral symmetry in Zr nuclei: Calculations of low-energy excitations with Gogny interaction. *J. Phys.* **G42** (2015) 015106.
19. N. S. Manton, Lightly bound Skyrmons, tetrahedra and magic numbers. [arXiv:1707.04073].
20. A. Heusler, Identification of rotating and vibrating tetrahedrons in the heavy nucleus ^{208}Pb . *Eur. Phys. J.* **A53** (2017) 215.
21. D. M. Dennison, Excited states of the O^{16} nucleus. *Phys. Rev.* **57** (1940) 454; Energy levels of the O^{16} nucleus. *Phys. Rev.* **96** (1954) 378.
22. S. L. Kameny, α -particle model of O^{16} . *Phys. Rev.* **103** (1956) 358.
23. D. Robson, Evidence for the tetrahedral nature of ^{16}O . *Phys. Rev. Lett.* **42** (1979) 876; Test of tetrahedral symmetry in the ^{16}O nucleus. *Phys. Rev.* **C25** (1982) 1108.
24. A.D. Frawley, J. D. Fox, L. C. Dennis, K. W. Kemper and N. R. Fletcher, Search for a 3^- state at 9.85 MeV excitation in ^{16}O via the $^{16}\text{O}(\alpha, \alpha')^{16}\text{O}^*(9.85 \text{ MeV})(\alpha_0)^{12}\text{C}$ angular correlation. *Phys. Rev.* **C27** (1983) 2482.
25. W. Bauhoff, H. Schultheis and R. Schultheis, Alpha cluster model and the spectrum of ^{16}O . *Phys. Rev.* **C29** (1984) 1046.
26. R. Bijker and F. Iachello, Evidence for tetrahedral symmetry in ^{16}O . *Phys. Rev. Lett.* **112** (2014) 152501.
27. C. J. Halcrow, C. King and N. S. Manton, Dynamical α -cluster model of ^{16}O . *Phys. Rev.* **C95** (2017) 031303(R).
28. T. H. R. Skyrme, A non-linear field theory. *Proc. Roy. Soc. Lond.* **A260** (1961) 127.
29. R. A. Battye, N. S. Manton and P. M. Sutcliffe, Skyrmons and the α -particle model of nuclei. *Proc. Roy. Soc. Lond.* **A463** (2007) 261.
30. P. H. C. Lau and N. S. Manton, Quantization of T_d - and O_h -symmetric Skyrmons. *Phys. Rev.* **D89** (2014) 125012.

22 *C. J. Halcrow, C. King and N. S. Manton*

31. D. M. Brink, H. Friedrich, A. Weiguny and C. W. Wong, Investigation of the alpha-particle model for light nuclei. *Phys. Lett.* **33B** (1970) 143.
32. C. J. Halcrow, *Skyrmions – Beyond Rigid Body Quantisation*. Ph.D. thesis, Cambridge University, 2017.
33. C. King, *$B = 4N$ Nuclei in the Skyrme Model*. Ph.D. thesis, Cambridge University, 2018.
34. J. I. Rawlinson, An alpha particle model for Carbon-12. *Nucl. Phys.* **A975** (2018) 122.
35. M. Freer and H. O. U. Fynbo, The Hoyle state in ^{12}C . *Prog. Part. Nucl. Phys.* **78** (2014) 1.
36. G. Herzberg, *Molecular Spectra and Molecular Structure: II. Infrared and Raman Spectra of Polyatomic Molecules*. Van Nostrand, Princeton NJ, 1945.
37. M. Johnston and D. M. Dennison, The interaction between vibration and rotation for symmetrical molecules. *Phys. Rev.* **48** (1935) 868.
38. D. Robson, Many-body interactions from quark exchanges and the tetrahedral crystal structure of nuclei. *Nucl. Phys.* **A308** (1978) 381.
39. Evaluated Nuclear Structure Data File, <https://www.nndc.bnl.gov/ensdf/index.jsp>.
40. L. D. Landau and E. M. Lifshitz, *Quantum Mechanics – Course of Theoretical Physics Vol. 3 (3rd ed.)*. Butterworth–Heinemann, Oxford, 1977.
41. F. A. Cotton, *Chemical Applications of Group Theory (3rd ed.)*. Wiley, New York, 1990.
42. P. C. Sood, Centrifugal stretching of a classical rotator and collective motions in nuclei. *Can. J. Phys.* **46** (1968) 1419.
43. E. Wold, The centrifugal stretching model and the deviation from the $L(L + 1)$ rule for rare-earth nuclei. *Nucl. Phys.* **A130** (1969) 650.
44. K. W. Kemper, G. G. Shute, C. H. Atwood, L. K. Fifield and T. R. Ophel, Spectroscopy of $A = 16$ from $^{13}\text{C}(^6\text{Li}, t)^{16}\text{O}$. *Nucl. Phys.* **A405** (1983) 348.
45. J. W. Bittner and R. D. Moffat, Elastic scattering of alpha particles by carbon. *Phys. Rev.* **96** (1954) 374.
46. M. Freer *et al.*, $^8\text{Be} + ^8\text{Be}$ decay of excited states in ^{16}O . *Phys. Rev.* **C70** (2004) 064311.
47. S. J. Sanders, L. M. Martz and P. D. Parker, Spectroscopy of high spin states in ^{16}O and ^{20}Ne using the $(^{12}\text{C}, ^8\text{Be})(\alpha_0)$ reaction. *Phys. Rev.* **C20** (1979) 1743.
48. L. L. Ames, Natural parity levels in ^{16}O . *Phys. Rev.* **C25** (1982) 729.
49. W. D. M. Rae, S. C. Allcock and J. Zhang, Spin assignments for states in ^{16}O using the $^{12}\text{C}(^{12}\text{C}, ^{16}\text{O}^*)^8\text{Be}$ transfer reaction. *Nucl. Phys.* **A568** (1994) 287.
50. M. Freer *et al.*, ^8Be and α decay of ^{16}O . *Phys. Rev.* **C51** (1995) 1682.

Appendix A

Table 1 lists all the quantum states below 20 MeV predicted by our model, and also those with spin 6 or more having energy less than 30 MeV. They are grouped into tetrahedral rovibrational bands.

Table 1: Bands of predicted quantum states. We tabulate for each state the spin/parity J^P , the underlying vibrational wavefunction on the E-manifold (displayed in Fig. 4), the vibrational energy $E_{\text{vib}} + n_A\omega_A + n_F\omega_F$, the rotational energy E_{rot} and total energy E (all in MeV).

Band	J^P	Vib. wvfn.	Vib. ener.	E_{rot}	E	
E ⁰	0 ⁺	ψ_{T0}^+	0	0	0	
	3 ⁻	ψ_{S0}^-	0.18	6.12	6.30	
	4 ⁺	ψ_{T0}^+	0	9.62	9.62	
	6 ⁺	ψ_{T0}^+	0	17.66	17.66	
	6 ⁻	ψ_{S0}^-	0.18	17.66	17.84	
	7 ⁻	ψ_{S0}^-	0.18	22.17	22.35	
	8 ⁺	ψ_{T0}^+	0	27.44	27.44	
	E ¹	2 ⁺	$u_1^+ \pm v_1^+$	3.45	2.54	5.99
		2 ⁻	$u_1^- \pm v_1^-$	5.27	2.54	7.81
4 ⁺		$u_1^+ \pm v_1^+$	3.45	7.42	10.87	
4 ⁻		$u_1^- \pm v_1^-$	5.27	7.42	12.69	
5 ⁺		$u_1^+ \pm v_1^+$	3.45	10.21	13.66	
5 ⁻		$u_1^- \pm v_1^-$	5.27	10.21	15.48	
6 ⁺		$u_1^+ \pm v_1^+$	3.45	13.04	16.49	
6 ⁻		$u_1^- \pm v_1^-$	5.27	13.04	18.31	
7 ⁺		$u_1^+ \pm v_1^+$	3.45	16.01	19.46	
7 ⁻		$u_1^- \pm v_1^-$	5.27	16.01	21.28	
8 ⁺		$u_1^+ \pm v_1^+$	3.45	19.52	22.97	
8 ⁺		$u_1^+ \pm v_1^+$	3.45	19.52	22.97	
8 ⁻		$u_1^- \pm v_1^-$	5.27	19.52	24.79	
8 ⁻		$u_1^- \pm v_1^-$	5.27	19.52	24.79	
9 ⁺		$u_1^+ \pm v_1^+$	3.45	24.46	27.91	
9 ⁻		$u_1^- \pm v_1^-$	5.27	24.46	29.73	
E ²		0 ⁺	ψ_{T2}^+	6.05	0	6.05
		2 ⁺	$u_2^+ \pm v_2^+$	8.72	2.54	11.26
	2 ⁻	$u_2^- \pm v_2^-$	11.05	2.54	13.59	
	3 ⁻	ψ_{S2}^-	10.67	4.80	15.47	
	4 ⁺	ψ_{T2}^+	6.05	7.42	13.47	
	4 ⁺	$u_2^+ \pm v_2^+$	8.72	7.42	16.14	
	4 ⁻	$u_2^- \pm v_2^-$	11.05	7.42	18.47	
	5 ⁺	$u_2^+ \pm v_2^+$	8.72	10.21	18.93	
	5 ⁻	$u_2^- \pm v_2^-$	11.05	10.21	21.26	
	6 ⁺	ψ_{T2}^+	6.05	13.04	19.09	
	6 ⁻	ψ_{S2}^-	10.67	13.04	23.71	
	6 ⁺	$u_2^+ \pm v_2^+$	8.72	13.04	21.76	
	6 ⁻	$u_2^- \pm v_2^-$	11.05	13.04	24.09	
	7 ⁺	$u_2^+ \pm v_2^+$	8.72	16.01	24.73	
	7 ⁻	$u_2^- \pm v_2^-$	11.05	16.01	27.06	
	7 ⁻	ψ_{S2}^-	10.67	16.01	26.68	
	8 ⁺	$u_2^+ \pm v_2^+$	8.72	19.52	28.24	
	8 ⁺	$u_2^+ \pm v_2^+$	8.72	19.52	28.24	
	8 ⁺	ψ_{T2}^+	6.05	19.52	25.57	
	E ³	0 ⁺	ψ_{T3}^+	14.89	0	14.89
		0 ⁻	ψ_{T3}^-	16.35	0	16.35
2 ⁺		$u_3^+ \pm v_3^+$	12.22	2.54	14.76	
2 ⁻		$u_3^- \pm v_3^-$	16.92	2.54	19.46	
3 ⁺		ψ_{S3}^+	12.57	4.80	17.37	
4 ⁺		$u_3^+ \pm v_3^+$	12.22	7.42	19.64	

24 *C. J. Halcrow, C. King and N. S. Manton*

E ⁴	0 ⁺	ψ_{T4}^+	18.78	0	18.78
F	1 ⁻	ψ_{T0}^+	6.55	0.57	7.12
	2 ⁺	ψ_{S0}^-	6.73	2.93	9.66
	3 ⁺	ψ_{S0}^-	6.73	4.66	11.39
	3 ⁻	ψ_{T0}^+	6.55	5.36	11.91
	4 ⁺	ψ_{S0}^-	6.73	6.58	13.32
	4 ⁻	ψ_{T0}^+	6.55	7.28	13.84
	5 ⁺	ψ_{S0}^-	6.73	11.12	17.85
	5 ⁻	ψ_{T0}^+	6.55	9.19	15.75
	5 ⁻	ψ_{T0}^+	6.55	11.12	17.67
	6 ⁺	ψ_{S0}^-	6.73	14.12	20.85
	6 ⁺	ψ_{S0}^-	6.73	12.90	19.63
	6 ⁻	ψ_{T0}^+	6.55	12.90	19.45
	7 ⁺	ψ_{S0}^-	6.73	14.64	21.38
	7 ⁺	ψ_{S0}^-	6.73	15.86	22.60
	7 ⁻	ψ_{T0}^+	6.55	14.64	21.20
	7 ⁻	ψ_{T0}^+	6.55	17.27	23.81
	8 ⁺	ψ_{S0}^-	6.73	17.98	24.72
	8 ⁺	ψ_{S0}^-	6.73	20.96	27.69
	8 ⁻	ψ_{T0}^+	6.55	19.38	25.94
8 ⁻	ψ_{T0}^+	6.55	20.96	27.51	
9 ⁻	ψ_{T0}^+	6.55	22.74	29.30	
A	0 ⁺	ψ_{T0}^+	12.05	0	12.05
	3 ⁻	ψ_{S0}^-	12.23	4.80	17.03
	4 ⁺	ψ_{T0}^+	12.05	7.42	19.47
E × F	1 ⁺	$u_1^- \pm v_1^-$	11.82	0.97	12.79
	1 ⁻	$u_1^+ \pm v_1^+$	10.00	0.97	10.97
	2 ⁺	$u_1^- \pm v_1^-$	11.82	2.12	13.94
	2 ⁻	$u_1^+ \pm v_1^+$	10.00	2.12	12.12
	3 ⁺	$u_1^- \pm v_1^-$	11.82	3.61	15.43
	3 ⁺	$u_1^- \pm v_1^-$	11.82	4.70	16.52
	3 ⁻	$u_1^+ \pm v_1^+$	10.00	3.61	13.61
	3 ⁻	$u_1^+ \pm v_1^+$	10.00	4.70	14.70
	4 ⁺	$u_1^- \pm v_1^-$	11.82	6.30	18.12
	4 ⁺	$u_1^- \pm v_1^-$	11.82	7.08	18.90
	4 ⁻	$u_1^+ \pm v_1^+$	10.00	6.30	16.30
	4 ⁻	$u_1^+ \pm v_1^+$	10.00	7.08	17.08
	5 ⁺	$u_1^- \pm v_1^-$	11.82	7.80	19.63
	5 ⁺	$u_1^- \pm v_1^-$	11.82	8.58	20.41
	5 ⁺	$u_1^- \pm v_1^-$	11.82	9.52	21.34
	5 ⁻	$u_1^+ \pm v_1^+$	10.00	7.80	17.81
	5 ⁻	$u_1^+ \pm v_1^+$	10.00	8.58	18.59
	5 ⁻	$u_1^+ \pm v_1^+$	10.00	9.52	19.52
6 ⁺	$u_1^- \pm v_1^-$	11.82	9.87	21.70	
6 ⁺	$u_1^- \pm v_1^-$	11.82	10.81	22.64	
6 ⁺	$u_1^- \pm v_1^-$	11.82	11.90	23.72	

Oxygen-16 Spectrum from Tetrahedral Vibrations and their Rotational Excitations 25

	6^-	$u_1^+ \pm v_1^+$	10.00	9.87	19.88
	6^-	$u_1^+ \pm v_1^+$	10.00	10.81	20.82
	6^-	$u_1^+ \pm v_1^+$	10.00	11.90	21.90
	7^+	$u_1^- \pm v_1^-$	11.82	11.99	23.82
	7^+	$u_1^- \pm v_1^-$	11.82	13.08	24.90
	7^+	$u_1^- \pm v_1^-$	11.82	14.33	26.15
	7^+	$u_1^- \pm v_1^-$	11.82	14.33	26.15
	7^-	$u_1^+ \pm v_1^+$	10.00	11.99	22.00
	7^-	$u_1^+ \pm v_1^+$	10.00	13.08	23.08
	7^-	$u_1^+ \pm v_1^+$	10.00	14.33	24.33
	7^-	$u_1^+ \pm v_1^+$	10.00	14.33	24.33
	8^+	$u_1^- \pm v_1^-$	11.82	14.55	26.38
	8^+	$u_1^- \pm v_1^-$	11.82	15.80	27.62
	8^+	$u_1^- \pm v_1^-$	11.82	15.80	27.62
	8^+	$u_1^- \pm v_1^-$	11.82	17.20	29.02
	8^-	$u_1^+ \pm v_1^+$	10.00	14.55	24.56
	8^-	$u_1^+ \pm v_1^+$	10.00	15.80	25.80
	8^-	$u_1^+ \pm v_1^+$	10.00	15.80	25.80
	8^-	$u_1^+ \pm v_1^+$	10.00	17.20	27.20
	9^-	$u_1^+ \pm v_1^+$	10.00	18.43	28.44
	9^-	$u_1^+ \pm v_1^+$	10.00	18.43	28.44
	9^-	$u_1^+ \pm v_1^+$	10.00	19.84	29.84
$E^2 \times F$	1^+	$u_2^- \pm v_2^-$	17.60	0.97	18.57
	1^-	$u_2^+ \pm v_2^+$	15.27	0.97	16.24
	1^-	ψ_{T2}^+	12.60	0.50	13.11
	2^+	ψ_{S2}^-	17.22	2.59	19.81
	2^+	$u_2^- \pm v_2^-$	17.60	2.12	19.72
	2^-	$u_2^+ \pm v_2^+$	15.27	2.12	17.39
	3^-	ψ_{T2}^+	12.60	4.70	17.30
	3^-	$u_2^+ \pm v_2^+$	15.27	3.61	18.88
	3^-	$u_2^+ \pm v_2^+$	15.27	4.70	19.97
F^2	0^+	ψ_{T0}^+	13.11	0	13.11
	1^-	ψ_{S0}^-	13.29	0.56	13.85
	2^+	ψ_{T0}^+	13.11	3.27	16.37
	2^+	ψ_{T0}^+	13.11	1.71	14.82
	2^-	ψ_{S0}^-	13.29	2.34	15.62
	3^+	ψ_{T0}^+	13.11	4.14	17.24
	3^-	ψ_{S0}^-	13.29	4.76	18.05
	3^-	ψ_{S0}^-	13.29	4.20	17.49
	4^+	ψ_{T0}^+	13.11	6.42	19.53
	4^+	ψ_{T0}^+	13.11	5.27	18.38
	4^-	ψ_{S0}^-	13.29	5.27	18.56
$E \times A$	2^+	$u_1^+ \pm v_1^+$	15.50	2.54	18.04
	2^-	$u_1^- \pm v_1^-$	17.32	2.54	19.86
$E^2 \times A$	0^+	ψ_{T2}^+	18.10	0	18.10